THREE PHASE CRYSTALLOGRAPHY AND SOLUTE DISTRIBUTION ANALYSIS DURING RESIDUAL AUSTENITE DECOMPOSITION IN TEMPERED NANOCRYSTALLINE BAINITIC STEELS

F. G. Caballero[1], Hung-Wei Yen[2,3], M. K. Miller[4], J. Cornide[1], Hsiao-Tzu Chang[2], C. Garcia-Mateo[1] and Jer-Ren Yang[2]

[1] Centro Nacional de Investigaciones Metalúrgicas (CENIM-CSIC), Avda Gregorio del Amo, 8; Madrid, E-28040, Spain

[2] Department of Materials Science and Engineering, National Taiwan University, 1, Roosevelt Rd. Sec. 4, Taipei 10617, Taiwan

[3] Australian Centre for Microscopy and Microanalysis, The University of Sydney, NSW 2006, Australia

[4] Oak Ridge National Laboratory (ORNL), Materials Science and Technology Division, Oak Ridge, TN 37831-6139, USA

Corresponding Author: Francisca G. Caballero.

Centro Nacional de Investigaciones Metalúrgicas (CENIM-CSIC), Avda Gregorio del Amo, 8; Madrid, E-28040, Spain.

Tf:+34 91 5538900

Fax: +34 91 5347425

Abstract

Interphase carbide precipitation due to austenite decomposition was investigated by high resolution transmission electron microscopy and atom probe tomography in tempered nanostructured bainitic steels. Results showed that cementite (θ) forms by a paraequilibrium transformation mechanism at the bainitic ferrite-austenite interface with a simultaneous three phase crystallographic orientation relationship.

Keywords: Steels, bainite, precipitation, atom probe tomography (APT)

1. Introduction

Many commercially successful steel concepts have been developed based on a mixed microstructure of bainitic ferrite (α) and carbon-enriched retained austenite (γ) [1-9]. The austenite is found to occur in two forms: as blocks (a few microns thick) of retained austenite located between the sheaves of bainite, and as fine 20-200-nm-thick films of austenite, which are retained between the subunits of a given sheaf of bainite. This retained austenite is not thermodynamically stable. There is ample evidence that austenite will decompose into a mixture of ferrite and carbides during tempering [1,4,10]. In order to accomplish cementite precipitation, the carbon content of the austenite should exceed that given by the extrapolated $\gamma/(\gamma+\theta)$ phase boundary.

The shape, size and carbon content of retained austenite play an important role in controlling its decomposition behavior. Coarse blocks of austenite tend to decompose into fine pearlite, whereas films of austenite decompose into discrete particles of cementite in a ferrite matrix, basically because they are too thin to permit the onset of the cooperative growth needed to establish a pearlite colony [11]. In addition, the nano-scale austenite films seem to be less stable than those with a sub-micron thickness, as recently revealed by in-situ high-energy synchrotron X-ray diffraction experiments [12,13]. This is because the nano-scale films of austenite are much more enriched in carbon and therefore have a higher driving force for cementite precipitation [14].

There is no partitioning of substitutional solutes across the bainitic ferrite-austenite interface during the bainite reaction, in spite of the requirements of equilibrium [15,16]. Thus, given the opportunity, substitutional elements are expected to redistribute

approaching equilibrium phase boundary as the bainite structure is tempered. Field ion microscopy and 1D atom probe revealed that when a mixture of bainitic ferrite and austenite is tempered at low temperature, the substitutional solutes partition before the austenite begins to decompose [17]. More recently, the compositional analysis of the austenite-bainitic ferrite interface by atom probe tomography (APT) [18] revealed chromium spikes at the austenite/bainitic ferrite interface indicating that negligible partitioning local equilibrium was reached. However, the retained austenite decomposed during tempering before equilibrium was reached at the interface.

It has long been known that cementite precipitation due to the decomposition of the residual austenite occurs at the austenite-bainitic ferrite interface. Hot-stage transmission electron microscopy (TEM) examination [19] of the precipitation events during tempering of an aggregate of retained austenite and bainitic ferrite formed at 350 °C for 205 min. in medium carbon high silicon steel, revealed that the majority of carbides formed at the austenite-bainitic ferrite interface and then grew into the austenite, so that the process of austenite decomposition can be described as interphase precipitation. Subsequently, the boundary pulled away from the line of carbides and this sequence continued repeatedly until the austenite had fully decomposed. In general, due to the thickness of the austenite film, only one or two lines of carbide were observed before austenite decomposition was completed [19]. That is the reason why a typical appearance of interphase precipitation in rows [20,21] is not observed at the nanoscale.

Austenite decomposition can also occur after the upper bainite transformation during an extensive aging, with a much longer time than is necessary to complete the bainite reaction. It is generally accepted that interlath carbide precipitation is a secondary event involving the diffusional decomposition of the carbon enriched austenite after bainitic

ferrite formation. Shackleton and Kelly [22] performed a systematic study of the crystallography of carbide precipitation in bainite. They found that the orientation relationships for interlath cementite in upper bainite were mainly constrained from the austenite. The observed α/θ relationships were derived assuming that the cementite precipitates from austenite with the Pitsch γ/θ relationship [23] and allowing the ferrite to be a variant of the Kurdjumov and Sachs α/γ relationship [24]. More recently, the following three-phase orientation relationship,

$$(111)_\gamma \parallel (011)_\alpha \parallel (\bar{1}03)_\theta \text{ and } [\bar{1}01]_\gamma \parallel [\bar{1}\bar{1}1]_\alpha \parallel [010]_\theta, \quad (1)$$

was considered in upper bainite structure of a Fe-Ni-C alloy [25], where the interlath cementite clearly nucleates at the austenite-ferrite boundary.

In the present work, the onset of interphase carbide precipitation due to the decomposition of the retained austenite was analyzed by the complementary techniques of high-resolution TEM (HRTEM) and APT in tempered nanostructured bainitic steels containing significant (20–40%) amounts of unstable austenite. The results have provided new experimental evidence on the crystallographic orientation relationships and solute distribution among the three phases (ferrite, austenite, and cementite) involved.

2. Material and methods

The chemical compositions of the studied steels are given in Table 1. The alloys were supplied after casting, rolling, and a homogenization heat treatment at 1200 ºC for 72 h.

Specimens were austenitized at 1000 ºC for 15 min. and then isothermally transformed at 200 ºC for 240 h before quenching into water. The microstructure thus obtained was tempered at temperatures below 400 ºC for different times. Previous X-ray diffraction (XRD) results suggest that the austenite should be fully decomposed after tempering at 450 ºC for 30 min. [26]. Details on the processing, heat treatments, and preliminary microstructural characterization of nanostructured bainitic steels are reported elsewhere [5,10,27].

Specimens for TEM were sliced from 3 mm diameter rods of tempered material, mechanically thinned to 0.06 mm, and then twin-jet electropolished to perforation with a mixture of 5% perchloric acid, 25% glycerol, and 70% ethanol at -5 °C at 40 V. The samples were examined on a Philips Tecnai F30 field emission gun (FEG) TEM operated at 300 keV.

APT specimens were cut from the tempered material and electropolished by standard micropolishing methods [28]. APT analyses were performed in the Cameca laser-assisted local electrode atom probe (LEAP 4000X HR), which was operated in voltage pulsed mode with a specimen temperature of 50 K, a pulse repetition rate of 200 kHz, and a pulse fraction of 0.2. The large field of view and rapid analysis capability of this instrument facilitated the analysis at an atomic scale of the nucleation of interphase carbides in steels. The solute distribution across the interphase interfaces was determined with proximity histograms [29]. The main advantages of this method are that it can accommodate the curvature of non-planar interfaces and enables solute profiles to be obtained that are normal to the interface.

3. Results and discussion

The initial microstructure of the steels studied consists of ~40 nm-thick plates of bainitic ferrite and 20-40% austenite, depending on the carbon and silicon content (Table 1) [30]. Retained austenite is enriched in carbon to 5-12 at. %, depending on its morphology and size. Nanoscale austenite films that were entrapped between neighboring subunits of bainitic ferrite have higher carbon contents than the submicron blocks of residual austenite located between the sheaves of bainite [14]. It is important to point out the high carbon content of the ferrite in nanostructured bainitic steels (~2.5 at. % C according to XRD data, is well above that expected from para-equilibrium with austenite to be 0.12 at.% C) [18] as well as the high dislocation density present in this phase [32]. This excess of carbon was found to be partly (~1 at. % C) in solid solution in the bainitic ferrite [33] and the remainder was trapped at dislocations [31,34]. Carbide particles within bainitic ferrite plates were not observed by TEM; however, cementite precipitation inside bainitic ferrite was identified in the initial microstructure by APT [16]. Bright-field TEM images and more details on the characterization of nanostructured bainitic steels are given elsewhere [16,18,30-34].

Tempering Steel1 at 400 ºC for 1 h did not change the hardness (~620 HV), suggesting negligible change in the initial microstructure. Extremely fine plates of ferrite and thin films of retained austenite were still observed. This treatment did not change the austenite volume fraction (~30%). Carbide precipitation due to austenite decomposition was not evident after TEM examination of this microstructure. Only a few carbide particles seemed to precipitate within the ferrite, as illustrated in the TEM image shown in Fig. 1a. APT confirmed the presence of ε-carbide, a part of lower bainite cementite

originally present in the initial microstructure, in ferrite for the same tempering temperature [35].

Direct imaging of austenite in Steel2 tempered at 400ºC for 4 h revealed interphase carbide precipitation, as shown in Fig. 1b. Carbide particles impinging with austenite-bainitic ferrite interfaces (see arrow pointing an example) were observed as an indication of the onset of austenite decomposition. Contrary to what was expected [36], the carbide does not seem to penetrate into the austenite. If the carbide nucleates at the interface and subsequently continues to grow into the austenite, it is not clear why it does not lie essentially within the austenite.

The corresponding HRTEM image in Fig. 2 revealed the nature of the carbide precipitation at the interface to be cementite. Cementite was identified by the appearance of (100) forbidden reflections [37] in the diffractogram calculated by the fast Fourier transformation (FFT) of the high resolution TEM image, as indicated by the circles in Fig. 2d. The most common carbide formed due to austenite decomposition is cementite, but there are notable exceptions, particularly in steels containing a large concentration of silicon. For instance, the (Fe,Si)C_x orthorhombic carbides reported by Schissler et al. [38] and the triclinic *c*-carbide discovered by Sandvik [39].

During austenite decomposition, new ferrite (α_{new}), also known as secondary ferrite [40], is formed together with cementite by the $\gamma \rightarrow \theta + \alpha_{new}$ reaction. Nakamura and Nagakura [40] proposed that this new ferrite grows by a displacive mechanism from the carbon depleted austenite. The regions of new ferrite were twinned, and this was explained as self-accommodating crystallographic variants of ferrite. By contrast, Bhadeshia [36] claimed that austenite films cannot decompose by further displacive ferrite formation due to *the incomplete reaction phenomenon* [41], which implies that

during bainite formation the carbon content of the austenite becomes enriched to such an extent that displacive transformation becomes thermodynamically impossible during subsequent tempering.

The three phase crystallographic analysis shown in Fig. 2 revealed that the bainitic ferrite and austenite hold the Kurdjumov-Sachs (K-S) orientation relationship (OR) [24]:

$$(011)_\alpha \parallel (111)_\gamma, \text{ and } [11\bar{1}]_\alpha \parallel [10\bar{1})_\gamma \quad (2)$$

In addition, the cementite particles hold approximately the Bagaryatsky OR [42] with the neighbouring bainitic ferrite and the new ferrite:

$$(100)_\vartheta \parallel (011)_\alpha, \text{ and } [010]_\theta \parallel [11\bar{1}]_\alpha \quad (3)$$

The Bagaryatsky OR is close to the Isaichev OR [43]:

$$(10\bar{3})_\vartheta \parallel (101)_\alpha, \text{ and } [010]_\theta \parallel [11\bar{1}]_\alpha \quad (4)$$

which are difficult to distinguish. Zhang and Kelly [44], by analyzing the Kikuchi line diffraction patterns, suggested that the Bagaryatsky OR might not exist.

Finally, the OR between cementite and austenite is close to the Pitsch OR [23]:

$$(100)_\vartheta \parallel (545)_\gamma, \text{ and } [010]_\theta \parallel [10\bar{1}]_\gamma \quad (5)$$

Howe and Spanos [45] also observed the Pitsch OR between cementite and austenite, but steps were evident on the interface. The formation of the steps has been explained by Zhang et al. [46] and Ye and Zhang [47]. They suggested that the steps come from the irrational OR and interface.

It is clear that the cementite attempts to minimize the interface energy by adopting an orientation variant and the three-phase crystallography that allows simultaneously matching cementite lattices with both, austenite and ferrite, adjacent phases. Accordingly, the results in Fig. 2 revealed that the following unique three phase crystallographic relationship was established among austenite, ferrite, and cementite at the interface, as strong evidence that the cementite is formed by interphase precipitation due to austenite decomposition:

$$[100]_\theta \parallel [011]_\alpha \parallel [111]_\gamma \quad (6)$$

$$[010]_\theta \parallel [11\bar{1}]_\alpha \parallel [10\bar{1}]_\gamma \text{ and} \quad (7)$$

$$[001]_\theta \parallel [\bar{2}1\bar{1}]_\alpha \parallel [\bar{1}2\bar{1}]_\gamma \quad (8)$$

Compositional analysis of interfaces formed during interphase carbide precipitation by APT is shown in Fig. 3. A carbon atom map with superimposed isoconcentration surfaces obtained from Steel1 tempered at 300 ºC for 30 min. is shown in Fig. 3a. The distribution of the carbon atoms in the analysis volume is not uniform and carbon-enriched and carbon-depleted regions are clearly distinguishable. This volume includes a carbon-enriched (~8 at. % C) austenite block and a bainitic ferrite plate (<1 at. % C) with dislocation tangles in the vicinity of the ferrite-austenite interface. Another example of a carbon atom map with superimposed isoconcentration surfaces showing

carbon trapped at dislocation tangles in bainitic ferrite in contact with austenite is reported elsewhere [33,48].

In addition, the proximity histogram across the interface in Fig. 3b reveals the presence of a 3-nm-thick carbide precipitate at the bainitic ferrite/austenite interface. The interphase carbide was identified as cementite based on the carbon concentration (~25 at. % C). It is also evident that carbon is depleted in the ferrite near the ferrite-cementite interface. The solute distribution, Fig. 3b, also shows a slight redistribution of silicon across the cementite interfaces, but there is no evidence for gross redistribution of chromium and manganese after tempering at 300 ºC for 30 min. Silicon, which is not usually found in cementite at equilibrium, is present during the early stage of tempering, and this is in agreement with previous research [49-51].

4. Summary

In summary, the onset of austenite decomposition during tempering of nanostructured bainitic steels was analysed by the use of HRTEM and APT. It was observed that cementite precipitates at the bainitic ferrite-austenite with a unique three phase crystallographic orientation relationship ensuring simultaneous lattice matching among the phases. Moreover, the compositional analysis of the interfaces indicated that cementite forms via a paraequilibrium transformation mechanism, but silicon soon diffuses out of the carbide during tempering.

Acknowledgements

Research was supported by ORNL's Shared Research Equipment (ShaRE) User Facility, which is sponsored by the Office of Basic Energy Sciences, Scientific User Facilities Division, U.S. Department of Energy. The authors also gratefully acknowledge the support of the Spanish Ministry of Science and Innovation for funding this research under the contract MAT2010-15330, respectively.

References

1. H.K.D.H. Bhadeshia, D.V. Edmonds, Bainite in Silicon Steels: New Composition-Property Approach. Part 1, Met. Sci., 17 (1983) 411-419.
2. H.K.D.H. Bhadeshia, D.V. Edmonds, Bainite in Silicon Steels: New Composition-Property Approach. Part 2, Met. Sci., 17 (1983) 420-425.
3. F.G. Caballero, H.K.D.H. Bhadeshia, K.J.A. Mawella, D.G. Jones, P. Brown, Design of novel high strength bainitic steels: Part 1, Mater. Sci. Technol., 17 (2001) 512-516..
4. F.G. Caballero, H.K.D.H. Bhadeshia, K.J.A. Mawella, D.G. Jones, P. Brown, Design of novel high strength bainitic steels: Part 2, Mater. Sci. Technol., 17 (2001) 517-522..
5. F.G. Caballero, H.K.D.H. Bhadeshia, Very strong bainite, Curr. Opin. Solid State Mater. Sci., 8 (2004) 251-257.
6. P.J. Jacques, Transformation-induced plasticity for high strength formable steels, Curr. Opin. Solid State Mater. Sci., 8 (2004) 259-265.
7. B.C. De Cooman, Structure-properties relationship in TRIP steels containing carbide-free bainite, Curr. Opin. Solid State Mater. Sci., 8 (2004) 285-303..

8. F.G. Caballero, M.J. Santofimia, C. García-Mateo, J. Chao, C.G. de Andrés, Theoretical design and advanced microstructure in super high strength steels, Mater. Des., 30 (2009) 2077-2083.
9. F.G. Caballero, S. Allain, J. Cornide, J.D. Puerta Velásquez, C. Garcia-Mateo, M.K. Miller, Design of cold rolled and continuous annealed carbide-free bainitic steels for automotive application, Mater. Des., 49 (2013) 667-680.
10. F.G. Caballero, H.K.D.H. Bhadeshia, K.J.A. Mawella, D.G. Jones, P. Brown, Very strong low temperature bainite, Mater. Sci. Technol., 18 (2002) 279-284.
11. H.K.D.H. Bhadeshia, Bainite in Steels. Transformations, Microstructure and Properties, Second ed., Institute of Materials, Minerals and Mining, London, 2001.
12. A.S. Podder, I. Lonardelli, A. Molinari, H.K.D.H. Bhadeshia, Thermal stability of retained austenite in bainitic steel: An in situ study, Proceedings of the Royal Society A: Mathematical, Physical and Engineering Sciences, 467 (2011) 3141-3156.
13. A. Saha Podder, H.K.D.H. Bhadeshia, Thermal stability of austenite retained in bainitic steels, Mater. Sci. Eng. A, 527 (2010) 2121-2128.
14. C. Garcia-Mateo, F.G. Caballero, M.K. Miller, J.A. Jimenez, On measurement of carbon content in retained austenite in a nanostructured bainitic steel, J. Mater. Sci., 47 (2012) 1004-1010.
15. H.K.D.H. Bhadeshia, A.R. Waugh, Bainite: An atom-probe study of the incomplete reaction phenomenon, Acta Metall., 30 (1982) 775-784.
16. F.G. Caballero, M.K. Miller, S.S. Babu, C. Garcia-Mateo, Atomic scale observations of bainite transformation in a high carbon high silicon steel, Acta Mater., 55 (2007) 381-390.

17. I. Stark, G.D.W. Smith, H.K.D.H. Bhadeshia, Distribution of substitutional alloying elements during the bainite transformation, Metall. Trans. A, 21 (1990) 837-844.
18. F.G. Caballero, M.K. Miller, C. Garcia-Mateo, C. Capdevila, S.S. Babu, Redistribution of alloying elements during tempering of a nanocrystalline steel, Acta Mater., 56 (2008) 188-199.
19. H.K.D.H. Bhadeshia, D.V. Edmonds, The bainite transformation in a silicon steel, Metall. Trans. A, 10 (1979) 895-907.
20. S. Mukherjee, I.B. Timokhina, C. Zhu, S.P. Ringer, P.D. Hodgson, Three-dimensional atom probe microscopy study of interphase precipitation and nanoclusters in thermomechanically treated titanium–molybdenum steels, Acta Mater. 61 (2013) 2521–2530.
21. Y.-J. Zhang, G. Miyamoto, K. Shinbo, T. Furuhara, Effects of α/γ orientation relationship on VC interphase precipitation in low-carbon steel, Scripta Mater. 69 (2013) 17-20.
22. D.N. Shackleton, P.M. Kelly, Morphology of Bainite, Physical properties of martensite and bainite. Special Report 93, Iron and Steel Institute, London, 1965.
23. W. Pitsch, Der Orientierungszusammenhang zwischen Zementit und Austenit, Acta Metall., 10 (1962) 897-900.
24. G. Kurdjumow, G. Sachs, Über den Mechanismus der Stahlhärtung, Z. Angew. Phys., 64 (1930) 325-343..
25. Y. Ohmori, Y.C. Jung, H. Ueno, K. Nakai, H. Ohtsubo, Crystallographic analysis of upper bainite in Fe-9%Ni-C alloys, Materials Transactions, JIM, 37 (1996) 1665-1671.

26. Garcia-Mateo C, Peet M, Caballero FG, Bhadeshia HKDH. Mater Sci Technol 2004;20:814.
27. C. Garcia-Mateo, M. Peet, F.G. Caballero, H.K.D.H. Bhadeshia, Tempering of hard mixture of bainitic ferrite and austenite, Mater. Sci. Technol., 20 (2004) 814-818.
28. M.K. Miller, Atom Probe Tomography: Analysis at the Atomic Level, Kluwer Academic / Plenum Publishers, 2000..
29. O.C. Hellman, J.A. Vandenbroucke, J. Rüsing, D. Isheim, D.N. Seidman, Analysis of three-dimensional atom-probe data by the proximity histogram, Microsc. Microanal., 6 (2000) 437-444.
30. T. Sourmail, F.G. Caballero, C. Garcia-Mateo, V. Smanio, C. Ziegler, M. Kuntz, R. Elvira, A. Leiro, E. Vuorinen, T. Teeri, Evaluation of potential of high Si high C steel nanostructured bainite for wear and fatigue applications, Mater. Sci. Technol., (2013). DOI: 10.1179/1743284713Y.0000000242.
31. I.B. Timokhina, H. Beladi, X.Y. Xiong, Y. Adachi, P.D. Hodgson, Nanoscale microstructural characterization of a nanobainitic steel, Acta Mater., 59 (2011) 5511-5522.
32. J. Cornide, G. Miyamoto, F.G. Caballero, T. Furuhara, M.K. Miller, C. Garcia-Mateo, Distribution of dislocations in nanostructured bainite, Solid State Phenom., 172-174 (2011) 117-122.
33. F.G. Caballero, M.K. Miller, C. Garcia-Mateo, Carbon supersaturation of ferrite in a nanocrystalline bainitic steel, Acta Mater., 58 (2010) 2338-2343.
34. F.G. Caballero, H.W. Yen, M.K. Miller, J.R. Yang, J. Cornide, C. Garcia-Mateo, Complementary use of transmission electron microscopy and atom probe

tomography for the examination of plastic accommodation in nanocrystalline bainitic steels, Acta Mater., 59 (2011) 6117-6123.

35. F.G. Caballero, M.K. Miller, C. Garcia-Mateo, Atom probe tomography analysis of precipitation during tempering of a nanostructured bainitic steel, Metall. Mater. Trans. A, 42 (2011) 3660-3668.
36. H.K.D.H. Bhadeshia, Lower Bainite Transformation And The Significance Of Carbide Precipitation, Acta Metall., 28 (1980) 1103-1114.
37. S. Nagakura, Y. Nakamura, T. Suzuki, Forbidden Reflection Intensity In Electron Diffraction And Its Influence On The Crystal Structure Image, Jpn J Appl Phys Part 2, V 21 (1982) 449-451.
38. J.M. Schissler, J. Arnould, G. Metauer, Investigation of the Decomposition of Postbainitic Austenite in Fe-1%C-4%Si Alloys During Isothermal Holding at 420 C. Effect of 1% Manganese Addition, 72 (1975) 779-793.
39. B.P.J. Sandvik, The Bainite Reaction in Fe-Si-C Alloys: The Secondary Stage, Metall. Trans. A, 13 (1982) 789-800.
40. T. Nakamura, S. Nagakura, Decomposition of Retained Austenite during the Tempering of Martensitic High Carbon Steel Studied by in situ Electron Microscopy, in: S. Japan Institute of Metals (Ed.) Int. Conf. on Martensitic Transformations (ICOMAT-86), 1986, pp. 386-391.
41. R.F. Hehemann, K.R. Kinsman, H.I. Aaronson, A debate on the bainite reaction, Metall. Trans. A, 3 (1972) 1077-1094.
42. Y.A. Bagaryatsky, Veroyatnue Mechanezm Raspada Martenseeta, Dokl. Akad. Nauk SSSR, 73 (1950) 1161-1164.Bagaryatsky YA. Dokl Akad Nauk SSSR 1950;73:1161.

43. I.V. Isaichev, Orientation between cementite and ferrite, Zhurnal Tekhnicheskoi Fiziki, 17 (1947) 835-838.
44. M.X. Zhang, P.M. Kelly, Crystallography of spheroidite and tempered martensite, Acta Mater., 46 (1998) 4081-4091.
45. J.M. Howe, G. Spanos, Atomic structure of the austenite-cementite interface of proeutectoid cementite plates, Phil. Mag. A, 79 (1999) 9-30.
46. W.-Z. Zhang, F. Ye, C. Zhang, Y. Qi, H.-S. Fang, Unified rationalization of the Pitsch and T–H orientation relationships between Widmanstätten cementite and austenite, Acta Mater. 48 (2000) 2209-2219.
47. F. Ye, W.-Z. Zhang, Coincidence structures of interfacial steps and secondary misfit dislocations in the habit plane between Widmanstätten cementite and austenite, Acta Mater. 50 (2002) 2761-2777.
48. E.V. Pereloma, I.B. Timokhina, J.J. Jonas, M.K. Miller, Fine-scale microstructural investigations of warm rolled low-carbon steels with and without Cr, P, and B additions', Acta Mater. 54 (2006) 4539-4551.
49. S.S. Babu, K. Hono, T. Sakurai, Atom-Probe Field-Ion Microscopy Study of the Partitioning of Substitutional Elements During Tempering of a Low-Alloy Steel Martensite, Metall. Mater. Trans. A, 25 (1994) 499-508.
50. R.C. Thomson, M.K. Miller, Carbide precipitation in martensite during the early stages of tempering Cr- andMo-containing low alloy steels, Acta Mater., 46 (1998) 2203-2213.
51. S.S. Babu, K. Hono, T. Sakurai, APFIM studies on martensite tempering of Fe-C-Si-Mn low alloy steel, Appl. Surf. Sci., 67 (1993) 321-327.

Table Captions:

Table 1: Chemical Composition of Nanocrystalline Bainitic Steels. The balance is Fe.

Figure Captions:

Figure 1: TEM images of tempered microstructures at: (a) 400 ºC for 1 h in Steel1 and (b) 400 ºC for 4 h in Steel2; the arrows indicate the position of cementite particles.

Figure 2: (a) HREM image of interphase precipitation of cementite at austenite/bainitic ferrite interface as revealed in Fig. 1b with a longer arrow; and corresponding live-fast Fourier transformation (FFT) diffractograms of (b) austenite, (c) bainitic ferrite, and (d) cementite. New ferrite (α_{new}) is also formed together with cementite by the reaction $\gamma \rightarrow \theta + \alpha_{new}$ during austenite decomposition. Black circles in (d) indicates (1 0 0) forbidden reflections.

Figure 3: (a) Carbon isoconcentration surfaces at 2.4 at.% C (red) and 6 at.% (blue) superimposed with the carbon atom map, and (b) proximity histograms across cementite (θ) precipitated at the ferrite (α)/austenite (γ) interface in Steel1 tempered at 300 ºC for 30 min.

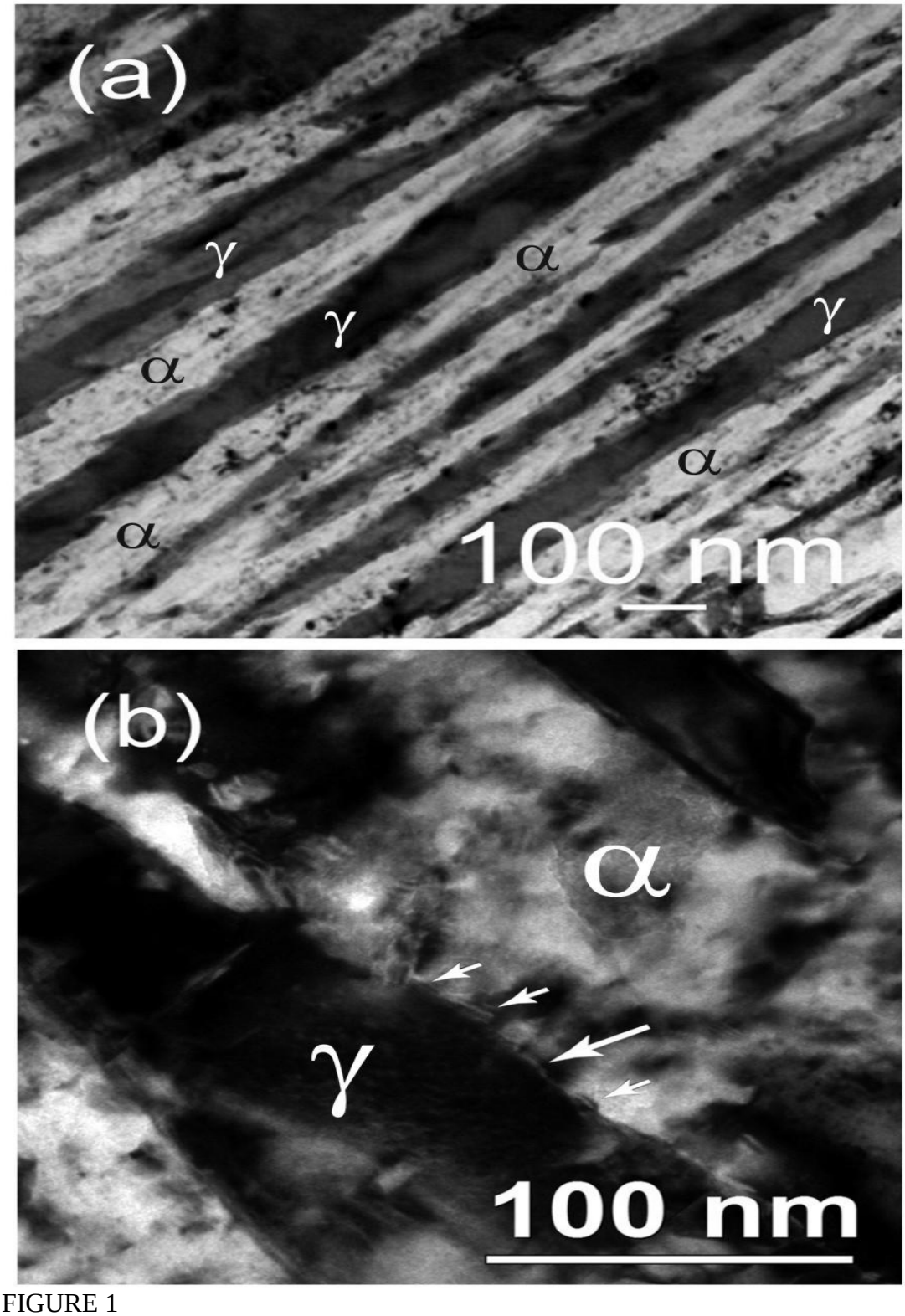

FIGURE 1

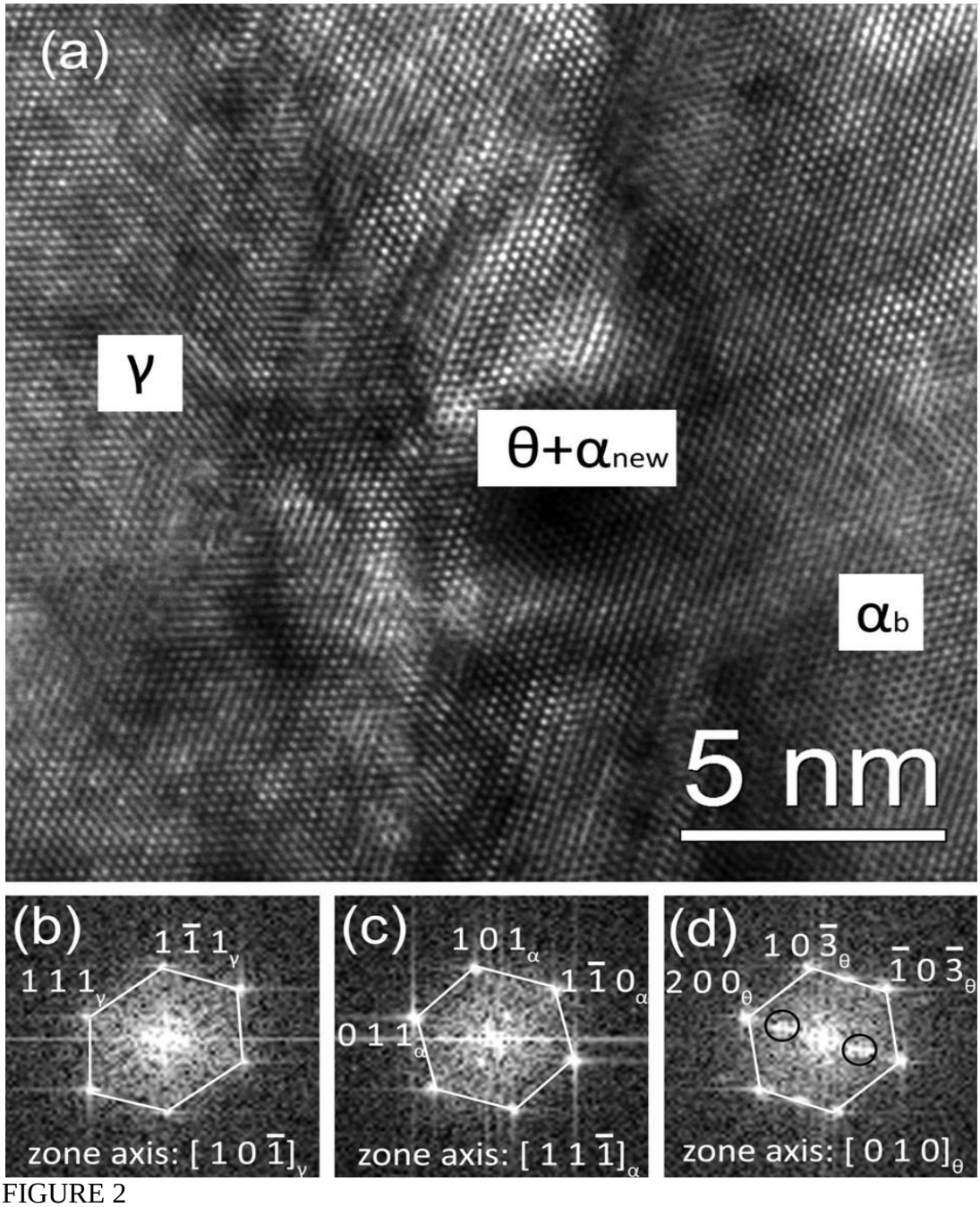
(a)
γ
θ+αnew
αb
5 nm
(b)
1 1 1γ
1 1̄ 1γ
zone axis: [1 0 1̄]γ
(c)
1 0 1α
1 1̄ 0α
0 1 1α
zone axis: [1 1 1̄]α
(d)
2 0 0θ
1 0 3̄θ
1̄ 0 3̄θ
zone axis: [0 1 0]θ

FIGURE 2

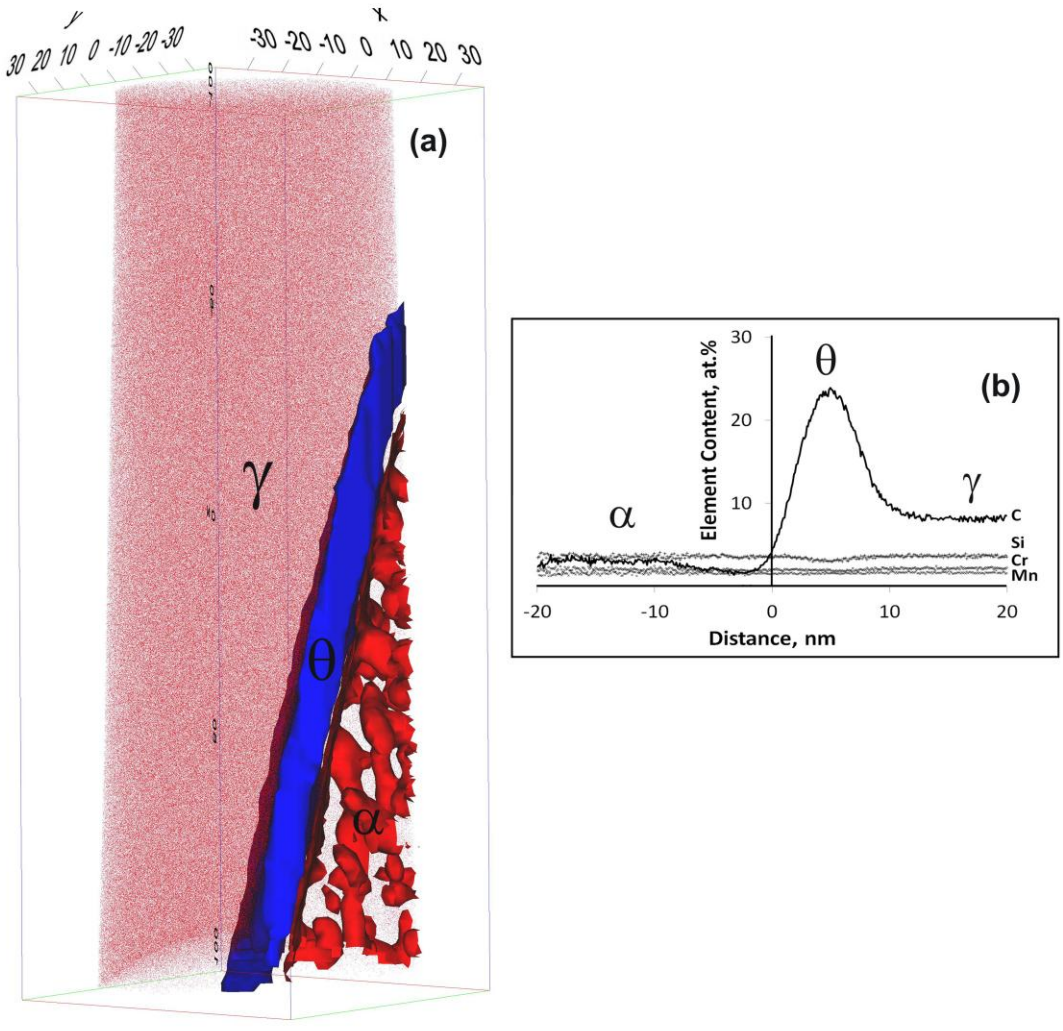

FIGURE 3

Table 1: Chemical Composition of Nanocrystalline Bainitic Steels. The balance is Fe.

Steel	C	Si	Mn	Mo	Cr	V
Steel1:						
wt%	1.0	1.5	1.9	0.3	1.3	0.1
at. %	4.3	2.8	1.8	0.1	1.3	0.1
Steel2:						
wt%	0.8	2.2	2.0	0.3	1.4	0.1
at. %	3.5	4.1	2.0	0.2	1.4	0.1

Highlights

- Interphase carbide precipitation due to austenite decomposition
- tempered nanostructured bainitic steels
- high resolution transmission electron microscopy and atom probe tomography
- paraequilibrium θ with three phase crystallographic orientation relationship.